Germinal center block exacerbates extrafollicular responses and accelerates autoimmune disease progression in a murine lupus model

Lasse F. Voss[1,2], Amanda J. Howarth[1], Thomas R. Wittenborn[1], Sandra Hummelgaard[1], Kristian Juul-Madsen[1], Kristian S. Kastberg[1], Mathias K. Pedersen[1], Lisbeth Jensen[1], Anastasios D. Papanastasiou[3], Thomas Vorup-Jensen[1], Kathrin Weyer[1], and Søren E. Degn[1*]

[1]Department of Biomedicine, Aarhus University, Aarhus, Denmark
[2]Department of Health Technology, Technical University of Denmark, Kongens Lyngby, Denmark
[3]Department of Biomedical Sciences, University of West Attica, Athens, Greece
[*]Corresponding author: sdegn@biomed.au.dk

Keywords: Autoimmunity, Germinal Centers, Extrafollicular Responses, B Cells, Autoantibodies, Systemic Lupus Erythematosus.

Abstract

Systemic lupus erythematosus and numerous other autoimmune diseases are characterized by affinity-matured, class-switched autoantibodies to nuclear antigens. Such antibodies are generally thought to arise in germinal centers (GCs). Several strategies to block GC formation and progression are currently being explored clinically. However, recent studies have suggested a key role for extrafollicular responses in driving the early events in autoimmune development. To investigate the relative contribution of these two pathways in autoimmune disease development, we leveraged a lupus murine model, where we could genetically block the GC pathway. We find that a B cell intrinsic block in GC formation accelerates extrafollicular responses and exacerbates autoimmune progression. The manifestations included higher levels of circulating, class-switched autoantibodies, as well as antibody- and complement-deposition in the kidney glomeruli. GC B cell cultures *in vitro* showed that loss of the GC transcription factor Bcl-6 prevents cellular expansion and accelerates plasma cell differentiation. This suggests that the *in vivo* phenotype was a direct consequence of rewiring of B cell intrinsic transcriptional programming. In a competitive scenario *in vivo*, in autoreactive mixed bone marrow chimeras, B cells harboring the genetic GC block contributed disproportionately highly to the plasma cell output. Taken together, this emphasizes the extrafollicular pathway as a key contributor to autoimmune pathogenesis and suggests that strategies aimed at blocking GCs should simultaneously target this pathway to avoid rerouting the pathogenic response.

Highlights:

-Genetic GC block exacerbates autoimmune progression in a lupus model
-An intrinsic GC block drives B cell differentiation into terminally differentiated plasma cells *in vitro*
-B cells harboring a GC block competitively contribute to the plasma cell compartment in an autoreactive setting *in vivo*
-Lupus mice with a GC block display immune complex deposition in kidney glomeruli that is indistinguishable from their wild-type counterparts

Introduction

Many autoimmune diseases, such as systemic lupus erythematosus (SLE) and Sjögren's syndrome, are characterized by the development of autoantibodies targeting nuclear antigens (Psianou et al., 2018; Rahman & Isenberg, 2008). Such antibodies can be produced by B cells via two routes, the extrafollicular pathway and the germinal center (GC) pathway (Elsner & Shlomchik, 2020). The extrafollicular pathway leads to the rapid expansion and differentiation of B cells to plasmablasts (PBs) and short-lived plasma cells (PCs), which in a natural infection setting provides rapid initial protection against pathogens. The GC pathway is slower, but enables a higher-quality response characterized by extensive somatic hypermutation and affinity maturation, robust memory cell generation, and production of long-lived PCs (Victora & Nussenzweig, 2012). At an individual B cell level, the decision between extrafollicular and GC pathway differentiation appears to rest on the initial affinity for antigen (Paus et al., 2006). While both pathways can support class-switch recombination and affinity maturation, the antibody class diversity and extent of somatic hypermutation is much greater through the GC pathway (Sweet et al., 2010; William et al., 2002).

Upon initial B cell activation by their cognate antigen, they can either T-independently or T-dependently form an extrafollicular focus. Here they proliferate, as well as potentially class-switch, and may additionally undergo a low degree of somatic hypermutation, before they differentiate into PCs. In the context of autoimmune diseases, it has been noted that initial B cell reactivities often target autoantigenic components that carry endogenous TLR ligands capable of stimulating them independently of T cells (Lau et al., 2005; Leadbetter et al., 2002; Sweet et al., 2011). Of note, these seem strictly limited to components topologically linked to the B cell receptor (Green et al., 2021). Interestingly, signals that drive initial B cell activation also seem to limit the extent of affinity maturation (Akkaya et al., 2018). However, as autoimmune disease progresses, the breadth of the autoantigenic response often broadens, leading to inclusion of T-dependent reactivities (Cornaby et al., 2015). In both humans and mice, this broadening of the response, termed epitope spreading, has been observed even before the onset of clinical symptoms (Arbuckle et al., 2003; Degn, van der Poel, Firl, et al., 2017).

Epitope spreading is thought to occur through the GC pathway. In this alternate outcome of initial B cell activation, the B cells may form a primary focus in the interfollicular region, where they undergo limited proliferation and may class-switch (Roco et al., 2019; Toellner et al., 1996). They then subsequently co-migrate with cognate T cells into the follicle, where they can form a GC. In the GC, the B cells proliferate rapidly and form a 'dark zone', and are now termed centroblasts (Victora & Nussenzweig, 2012). The centroblasts undergo somatic hypermutation to diversify their B cell receptors. They subsequently migrate to the 'light zone', where they scan follicular dendritic cells for antigen. The B cells that display the highest affinity for antigen can competitively acquire antigen and present derived peptides to T follicular helper (T_{FH}) cells. B cells that receive cognate T cell help may return to the dark zone for another round of division and hypermutation. B cells that do not receive help perish through programmed cell death and are engulfed by tingible body macrophages (Victora & Nussenzweig, 2012). Due to the power of the GC pathway, and the risk for inadvertent emergence of novel (auto)reactivities that are distinct from the original antigenic target, it is subject to stringent control. The requirement for T cell selection subsequent to every successive round of hypermutation, a phenomenon termed linked recognition, restricts

inadvertent broadening of the response. An additional layer of control appears to be exerted by a specialized subset of T regulatory cells, termed T follicular regulatory (T_{FR}) cells (Fahlquist Hagert & Degn, 2020). Nonetheless, these mechanisms appear to fail in autoimmune disease, which frequently display rampant GC activity (Domeier et al., 2017; Luzina et al., 2001).

Hence, we hypothesized that the GC pathway is critical to the autoimmune process, and that a genetic block of the GC pathway *in vivo* would prevent autoimmune development. To our surprise, a global block in the GC pathway *in vivo* did not ameliorate autoimmune disease, but rather exacerbated it. In an *in vitro* GC B cell culture system, GC blocked B cells expanded to a lesser extent, but were found to more rapidly develop into PBs and PCs. In a competitive scenario *in vivo*, GC blocked B cells competed efficiently with their wild-type counterparts, disproportionate to their inability to participate in GCs. Our determination of the relative contributions of the extrafollicular and GC pathways to autoimmune progression highlight a critical role of extrafollicular responses in driving autoimmune development.

Materials and methods

Mice

The Bcl-6$^{flx/flx}$ strain (Hollister et al., 2013) and congenic B6.CD45.1 (B6.SJL-Ptprc^{a} Pepc^{b}/BoyJ) were purchased from Jackson Laboratories (stock no. 023737 and 002014, respectively). Aicda-Cre transgenic mice (Kwon et al., 2008) were kindly provided by Meinrad Busslinger, The Research Institute of Molecular Pathology (IMP), Vienna. Aicda-Cre and Bcl-6$^{flx/flx}$ strains were intercrossed to generate Aicda-Cre+ and Aicda-Cre- Bcl-6$^{flx/flx}$ littermates. 564Igi mice (Berland et al., 2006) (B6.Cg-Igh$^{tm1(Igh564)Tik}$Igk$^{tm1(Igk564)Tik}$/J) were kindly made available by Theresa Imanishi-Kari, Tufts University, and provided by Michael C. Carroll, Boston Children's Hospital. Mice were housed in the Animal Facility at the Department of Biomedicine, Aarhus University, Denmark, under specific pathogen-free (SPF) conditions, on a 12-hour light/dark cycle with standard chow and water *ad libitum*. Both male and female mice were used in experiments. Mice were between 8 and 14 weeks old upon initiation of experiments.

Ethics Statement

All animal experiments were conducted in accordance with the guidelines of the European Community and were approved by the Danish Animal Experiments Inspectorate (protocol numbers 2017-15-0201-01348 and 2017-15-0201-01319).

R848 treatment protocol

Mice were treated topically on the right ear 3 times per week for 4 weeks with 1 mg R848/mL acetone using a cotton applicator or did not receive any treatment (Untreated/Unt).

Mixed bone marrow chimeras

Recipient mice were irradiated with 9 Gy in a MultiRad 350 (Faxitron), with 350 kV, 11.4 mA, a Thoraeus filter [0.75 mm Tin (Sn), 0.25 mm Copper (Cu), and 1.5 mm Aluminium (Al)], and with a beam-distance of 37 cm. Irradiated recipients were kept on antibiotic water (either 1 mg sulfadiazine together with 0.2 mg trimethoprim per mL drinking water, or 0.25 mg amoxicillin per mL drinking water) to avoid any opportunistic infections. On the following day, donor mice were anesthetized with 4% isoflurane and euthanized. Femora, fibulae/tibiae, ossa coxae and humeri were harvested, mechanically cleaned and rinsed in FACS buffer. The Bone marrow (BM) cells were released from the harvested bones by crushing and the cell extract was then passed through a 70 µm cell strainer. The donor BM cells were then counted in a Cellometer K2 cell counter (Nexcelom). Cells were pelleted by centrifugation (200 *g*, 10 min, 4°C) and resuspended to $1*10^{8}$ cells/mL. Donor cells from three different mice were then mixed according to the proportions mentioned in the figure legend. The donor cell mixtures were used to reconstitute the recipient mice by retroorbital injection of 200 µL (containing a total of $20*10^{6}$ cells) into each recipient mouse. The reconstituted recipient mice were placed on antibiotic water the following 14 days.

Tissue preparation

Mice were anesthetized with isoflurane (055226, ScanVet), blood samples from the retroorbital plexus were collected, and mice were euthanized using 100-150 mg/kg sodium pentobarbital (450009, Dechra Veterinary Products). Mesenteric lymph nodes (MesLN) and inguinal lymph nodes (IngLN) were removed, the splenic artery was clamped with a hemostat, and the spleen was removed. The mice were perfused intracardially with PBS (BE17-515Q,

159 Lonza) to remove the blood, and subsequently perfused with 4% w/v paraformaldehyde (PFA)
160 (1.04005.100, Merck) in PBS to fix the tissues. Finally, kidneys and auricular lymph nodes
161 (AurLNs) were removed.
162 Collected blood samples were centrifuged at 3,000 *g* for 10 minutes, the supernatant
163 was collected, and centrifuged again at 20,000 *g* for 3 minutes. Serum samples were stored
164 at -20°C. The spleen and AurLNs was directly embedded in Tissue-Tek O.C.T. media (4583,
165 Sakura Finetek) and frozen at -20°C for histology. The kidneys were kept in 4% w/v PFA for 24
166 hours, and then changed to 30% w/v sucrose in PBS. A small part of the spleen as well as IngLN
167 and MesLN were stored in fluorescence-associated cell sorting (FACS) buffer (PBS, 2% heat-
168 inactivated fetal calf serum (FCS), 1 mM ethylenediaminetetraacetic acid (EDTA)) for FACS
169 typing.
170
171 **Flow cytometry**
172 Spleen, IngLN and MesLN were harvested, stored into ice-cold FACS buffer, and mechanically
173 dissociated using pestles. Spleen and LNs were filtered through 70 μm cell strainers. Spleen
174 samples were centrifuged at 200 *g* for 5 minutes at 4°C, lysed in RBC lysis buffer (155 mM
175 NH_4Cl, 12 mM $NaHCO_3$, 0.1 mM EDTA), incubated at RT for 3 minutes, centrifuged, and finally
176 resuspended in FACS buffer or calcium-containing buffer (PBS, 20 mM HEPES, 145 mM NaCl,
177 5 mM $CaCl_2$, 2% FBS) when Annexin-V was included in the panels. Samples were filtered
178 through 70 μm cell strainers. Twenty μL Fc-block (553142, BD) diluted 1:50 in PBS and 100 μL
179 of each sample was added onto a 96-well plate and incubated for 5-10 minutes. Antibodies
180 and fixable viability dye (65-0865-14, ThermoFisher Scientific) were diluted in FACS buffer or
181 calcium-containing buffer as indicated below. One hundred μL antibody mix was added to
182 each sample well and incubated for 30 minutes on ice. The plate was centrifuged at 200 *g* for
183 5 minutes, supernatant was removed, and cells were fixed for 30 minutes in PBS, 0.9%
184 formaldehyde (F1635, Sigma- Aldrich) at RT. Later, the plates were centrifuged at 200 *g* for 5
185 minutes, the supernatant discarded, and the samples resuspended in FACS buffer or calcium-
186 containing buffer. Flow cytometry evaluation was performed the following day using a 4-laser
187 (405 nm, 488 nm, 561 nm, 640 nm) LSRFortessa analyzer (BD instruments). The following
188 antibodies and reagents were used for flow cytometry experiments: Annexin-V-AF488
189 (A13201, ThermoFisher Scientific, 1:500), B220-PB clone RA3-6B2 (558108, BD, 1:500), B220-
190 PerCP-Cy5.5 clone RA3-6B2 (561101, BD Biosciences, 1:500), CD4-PerCP clone RM4-5
191 (100538, BioLegend, 1:500), CD8-PerCP-Cy5.5 clone SK1 (565310, BD, 1:500), CD38-PE-Cy7
192 clone 90 (102718, BioLegend, 1:500), CD45.1-FITC clone A20 (110706, BioLegend, 1:500),
193 CD45.2-APC clone 104 (109814, BioLegend, 1:500), CD95-PE clone Jo2 (554258, BD, 1:500),
194 CD138-BV650 clone 281-2 (564068, BD, 1:500), 9D11-biotin (hybridoma kindly provided by
195 Elisabeth Alicot, Boston Children's Hospital, produced, purified and biotinylated in-house,
196 1:300), Ly6G/C-APC-R700 clone RB6-8C5 (565510, BD, 1:500), Viability Dye eFlour 780 (65-
197 0865-14, Thermo Fisher Scientific, 1:2000), Streptavidin-BV786 (563858, BD Biosciences,
198 1:500), hCD2-PB clone RPA-2.10 (300236, BioLegend, 1:200), IgD-AF488 clone 11-26c.2a
199 (405718, BioLegend, 1:500), IgMb-BV510 clone AF6-78 (742344, BD OptiBuild, 1:500), TACI-
200 AF647 clone 8F10 (558453, BD Biosciences, 1:500), CD45.2-BV786 clone 104 (563686, BD
201 Horizon, 1:500), CD19-AF700 clone 1D3 (557958, BD Pharmingen, 1:500).
202
203 **Quantum Dot coupling of antibody**
204 Quantum Dot (QD) antibody coupling was done using SiteClick Qdot 655 Antibody Labeling
205 Kit (Molecular Probes, S10453) according to manufactures instructions. In brief, antibody

206 (either “14D12” rat IgG2a to mouse MBL-C (Hycult Biotech), or “RTK2758” rat IgG2a isotype
207 control (Abcam)) was concentrated in antibody preparation buffer to a concentration of 2
208 mg/mL or above. Next, carbohydrates on the antibody were modified by the incubation with
209 β-galactosidase for 4 h at 37°C. Azide modification was achieved through incubation with
210 uridine diphosphate glucose-GalT enzyme overnight at 30°C. Antibody with modified
211 carbohydrates was purified and concentrated through a series of centrifugation steps using a
212 molecular-weight cutoff membrane concentrator, and the buffer was simultaneously
213 changed to 20 mM Tris, pH 7.0. Finally, 5’-dibenzocyclooctyne-modified QD nanocrystals were
214 coupled overnight at 25°C and stored at 4°C until further use.
215
216 **Nanoparticle Tracking Analysis**
217 Samples for Nanoparticle Tracking Analysis (NTA) were analyzed using a NanoSight NS300
218 system (Malvern Panalytical) as previously described (Juul-Madsen et al., 2021). The system
219 was configured with a 405 nm laser, a high-sensitivity scientific complementary metal–oxide–
220 semiconductor Orca Flash 2.8/Hamamatsu C11440 camera (Malvern Panalytical), a syringe
221 pump, and for fluorescence measurements, a 650 nm long-pass filter was used. The sample
222 chamber was washed twice with 1 mL PBS with 1 mM EDTA (PBS/EDTA) before each
223 measurement. All samples were thoroughly mixed before measurement and were injected
224 into the sample chamber using 1-mL syringes. The measurement script comprised
225 temperature control at 23°C, followed by a 20 s flush at a flowrate mark 1000. Next, sample
226 advancement was stabilized by a 120 s advancement at flowrate mark 10. Recordings were
227 captured continuously during a steady flow at flowrate mark 10 with five 60-s recordings
228 separated by 5-s lag time between each sample. The videos were collected and analyzed using
229 NanoSight software (version 3.4 with a concentration upgrade; Malvern). Automatic settings
230 were used for the minimal expected particle size, minimum track length, and blur setting.
231 Camera sensitivity and detection threshold were adjusted according to sample composition
232 and kept constant for all samples to be directly compared. For fluorescence mode, the camera
233 level was set to maximum (mark 16), and the detection threshold was set to minimum (mark
234 2). Serum samples from mice were analyzed in a 1:20 dilution in PBS/EDTA with a 1:20,000
235 dilution of MBL-C–specific (14D12) or isotype Antibody-QD reporters. A 50 nm cutoff was
236 established for all samples to exclude unbound QD conjugates as well as QD conjugates bound
237 to smaller forms of MBL-C.
238
239 **Immunohistochemical labelling of kidney tissue**
240 After perfusion fixation, kidneys were stored in PBS with 30% sucrose and 0.1% sodium azide.
241 For paraffin-embedding, the kidneys were washed in 10 mM PBS several times, dehydrated
242 in 70%, 96%, and 99% ethanol for 2 hours, respectively, before they were transferred to
243 xylene overnight. The day after, kidneys were embedded in paraffin. Paraffin embedded
244 kidney sections (2 µm) were cut on a Leica RM 2165 microtome (Leica, Wetzlar, Germany)
245 and dried at 60°C for 1 h. For immunofluorescent (IF) labelling, sections were placed in xylene
246 overnight, rehydrated in graded alcohols, and heated in TEG buffer (10 mM Tris, 0.5 mM EGTA
247 buffer, pH 9) at ~100°C for 10 min to induce epitope retrieval. Sections were subsequently
248 cooled for 30 min, incubated in 50 mM NH_4Cl in 0.01 mM PBS for 30 min, and incubated at
249 4°C with primary antibody overnight. The following day, sections were washed, incubated
250 with secondary antibody for 1 h, and coverslips were mounted using mounting medium (Dako
251 fluorescence Mounting medium, #S3023). Immunofluorescent images were acquired by a
252 confocal laser-scanning microscope (LSM 800 with Airyscan, Carl Zeiss GnHb, Jena, Germany)

253 and processed using ZEN lite 3.4 (Blue edition). For immunoperoxidase (IP) labelling, sections
254 were prepared as stated above. In addition, endogenous peroxidase was blocked by placing
255 sections in 30% H_2O_2 in methanol for 30 min and peroxidase-conjugated secondary antibodies
256 were used. Furthermore, the sections were incubated with DAB, counterstained with Mayer's
257 haematoxylin (Sigma-Aldrich), dehydrated in graded alcohols, cleared in xylene and mounted
258 with coverslips using Eukitt. For periodic acid-Schiff (PAS) stainings, sections were incubated
259 in 1% periodic acid for 10 min and treated with Schiff's reagent for 20 min. Subsequently, all
260 sections were counterstained with Mayer's hematoxylin for 5 min and mounted with
261 coverslips using Eukitt. Peroxidase-labelled and PAS-stained images were collected by a Leica
262 DFC320 camera (Leica, Wetzlar, Germany). H&E and PAS stained kidney sections were scored
263 by a histopathologist, blinded to the identity of the samples. High-resolution images of kidney
264 and spleen sections were obtained using a Zeiss LSM 800 Airyscan confocal microscope with
265 4 lasers (405 nm, 488 nm, 561 nm, 640 nm). ZEN software was used for quantification of
266 immunofluorescence kidney stainings. The following primary antibodies were used: anti-C3
267 (ab11887, Abcam, 1:25 (IP), 1:50 (IF)), anti-IgG2c (1079-08, SouthernBiotech, 1:25 (IF), 1:50
268 (IP)), anti-Nephrin (GP-N2, Progen, 1:100), anti-Ig (1010-08, SouthernBiotech, 1:100 (IF),
269 1:200 (IP)). The following secondary antibodies were used: Donkey-a-rabbit AF488 (A21206,
270 ThermoFisher, 1:300), Streptavidin AF647 (405237, BioLegend, 1:500), Goat-a-Guinea Pig
271 AF488 (A11073, ThermoFisher, 1:300), Goat-a-rabbit HRP (P0448, Dako, 1:200), Streptavidin
272 HRP (P0397, Dako, 1:200)
273
274 **Time-resolved immunofluorometric analysis (TRIFMA) anti-dsDNA measurements**
275 A FluoroNunc Maxisorp 96-well plate was coated with 100 µg/mL salmon sperm dsDNA
276 (AM9680, Invitrogen) in PBS and incubated overnight at 4°C. Wells were blocked with 200 µL
277 TBS containing 1% bovine serum albumin (BSA) (A4503, Sigma-Aldrich) for 1 hour at RT and
278 washed 3 times with TBS/Tw (TBS containing 0.05% v/v Tween-20 (8.17072.1000, Merck)).
279 Samples, standards and quality controls were diluted in TBS/Tw containing 5 mM EDTA and
280 0.1% w/v BSA, and were subsequently loaded onto the plate in duplicates. The plate
281 incubated at 37°C for 1 hour. Then, wells were washed 3 times in TBS/Tw and incubated with
282 biotinylated antibody (Table 2.5) at 37°C for 1 hour. Wells were washed 3 times in TBS/Tw,
283 and Eu^{3+}-tagged streptavidin (1244-360, PerkinElmer) diluted 1:1,000 in TBS/Tw containing
284 25 µM EDTA were subsequently added to the wells and incubated at RT for 1 hour. Finally,
285 the wells were washed 3 times in TBS/Tw, 200 µL enhancement buffer (AMPQ99800,
286 Amplicon) was added. The plate was shaken for 5 minutes and counts were read by a time-
287 resolved fluorometry plate reader Victor X5 (Perkin Elmer).
288
289 **TRIMA Ig measurements**
290 A FluoroNunc Maxisorp 96-well plate was coated with 1 µg/mL goat anti-mouse Ig in PBS and
291 incubated overnight at 4°C. Wells were blocked in 1 mg HSA/mL TBS for 1 hour at RT and
292 washed 3 times with TBS/Tw. Samples, standards and quality controls, diluted in TBS/Tw
293 containing 100 µg/mL heat-aggregated human Ig, were subsequently loaded onto the plate
294 in duplicates, and incubated overnight at 4°C. The wells were washed 3 times with TBS/Tw,
295 and 1 µg/mL biotinylated goat anti-mouse Ig was added to the wells and incubated for 2 hours
296 at RT. Wells were washed 3 times in TBS/Tw, and Eu^{3+}-tagged streptavidin (1244-360,
297 PerkinElmer) diluted 1:1,000 in TBS/Tw containing 25 µM EDTA were subsequently added to
298 the wells and incubated at RT for 1 hour. Finally, the wells were washed 3 times in TBS/Tw,
299 200 µL enhancementbuffer (AMPQ99800, Amplicon) was added. The plate was shaken for 5

300 minutes and counts were read by a Victor X5 time-resolved fluorometry plate reader (Perkin
301 Elmer).
302
303 **Immunofluorescence staining of spleens and auricular lymph nodes**
304 A Cryostar NX70 Cryostat (ThermoFisher) was used to cut 16 µm thick spleen sections or 20
305 µm thick auricular lymph node sections which were mounted on SuperFrost+ glass slides
306 (Fisher Scientific). Spleen sections were either acetone or PFA fixed, auricular lymph nodes
307 were PFA fixed. For acetone fixation, the spleen samples were rinsed in PBS and fixed in
308 acetone for 10 minutes at room temperature (RT), whereafter the slides were rehydrated in
309 PBS for 3 minutes. For PFA fixation protocols, the slides were washed in PBS, fixed with 4%
310 w/v PFA for 30 min at RT, incubated in TBS (10 mM Tris, 140 mM NaCl, pH 7.4) for 30 min at
311 RT, rinsed briefly with PBS, and incubated with permeabilization buffer (PBS, containing 2%
312 v/v FBS, 0.1% w/v sodium azide, 0.1% v/v Triton-X100) for 45 minutes at RT. Antibodies were
313 diluted in staining buffer (PBS, 2% v/v FBS, 0.1% w/v sodium azide). The antibody mix was
314 centrifuged at 10,000 *g* for 5 minutes and added onto the spleen samples, where it incubated
315 overnight at 4°C. The slides were washed once with staining buffer for 5 minutes and washed
316 3 times in PBS with 0.01% v/v Tween-20 for 5 minutes. Slides were spot-dried and mounted
317 using Fluorescence Mounting Medium (S3023, Dako). Imaging for quantification of GC
318 formation was performed using an Olympus VS120 Upright Widefield fluorescence slide
319 scanner equipped with a digital monochrome camera (Hamatsu ORCA Flash4.0V2) and a 2/3"
320 CCD camera, as well as single-band exciters and a filter wheel with single-band emitters
321 (Hoechst, FITC, Cy3, Cy5, and Cy7). Fiji v. 2.1.0/1.53c was used for image processing. The
322 following antibodies were used: CD45.1-FITC clone A20 (110706, BioLegend, 1:300), CD45.2-
323 APC clone 104 (109814, BioLegend, 1:300), CD138-PE clone 281-2 (142504, BioLegend, 1:500),
324 CD169-PE clone 3D6.112 (142404, BioLegend, 1:500), IgD-AF488 clone 11-26c.2a (405718,
325 BioLegend, 1:500), Ki67-eflour660 clone SolA15 (50-5698-82, Thermo Fisher Scientific, 1:500),
326 CD21/35-PB clone 7E9 (123414, BioLegend, 1:500). Channel intensities were adjusted for
327 visual clarity in represented micrographs, but quantification was performed on raw images
328 throughout.
329
330 **Purification of B cells**
331 The spleen was harvested, stored in MACS buffer (PBS, 2% FBS, 2 mM EDTA), the cells were
332 mechanically dissociated and filtered through 70 µm cell strainers, whereafter the cell
333 suspension was topped up with MACS buffer until 25 mL and filtered through 70 µm cell
334 strainers again. The cell suspension was centrifuged at 200 *g* for 10 minutes at 4°C,
335 resuspended in 5 mL RBC lysis buffer (155 mM NH_4Cl, 12 mM $NaHCO_3$, 0.1 mM EDTA), and
336 incubated for 3 minutes at RT. The reaction was stopped by adding 47 mL MACS buffer, and
337 centrifuged at 200 *g* for 5 minutes at 4°C. The supernatant was discarded and resuspended in
338 3 mL MACS buffer. B cell kit (Miltenyi Biotec, 130-090-862) was followed according to the
339 manufacturer's protocol.
340
341 **iGB cultures**
342 NB21 feeder cells, kindly provided by Garnett Kelsoe, Duke University (Kuraoka et al., 2016),
343 were seeded into 6-well plates at a density of 520 cells/cm^2 for IL-4 stimulated wells and 5200
344 cells/cm^2 for the four other conditions. The following day (day 0), B cells were purified
345 according to the described protocol, and resuspended in B cell medium (BCM) (RPMI-1640
346 supplemented with 10% FCS, 55 µM 2-ME, 1% Pen/Strep, 1% MEM NEAA, 10 mM HEPES, 1

347 mM Sodium Pyruvate). B cells were pre-diluted in BCM with the given cytokine cocktail as
348 indicated in figure legends. From day 2-8, 2/3 of the total volume of BCM was collected and
349 fresh BCM was added to reach the same final volume. One mL of medium from each well of
350 the 6 well plates was collected on the final day (day 10) for TRIFMA analyses. Cells were
351 analyzed using flow cytometry, as described above. IL-4 (214-14, PeproTech) were used for
352 stimulation
353
354 **Statistical analyses**
355 GraphPad Prism v. 8.4.3 was used for statistical analyses. For each dataset, both tests for
356 normality (such as Shapiro Wilk's test) and Q-Q plots were used to determine whether the
357 data were normally distributed. Data that were not normally distributed were log-
358 transformed and re-tested for normality. The following data sets were log-normally
359 distributed: Fig 1B, 1D, 1E, 1N (all 3 data sets), 1P (all 3 data sets), 3F, 5F, 5G, 5H. All other
360 datasets were normally distributed, except for the data in Figure 1L and 5F, which were
361 neither normally, nor log-normally distributed. However, a non-parametric t-test for the
362 isolated data of between each group in panel 1L and 5F showed similar results (for Fig 1L: a
363 significant increase in GC formation in Cre- between Unt and R848. For Fig 5F: a significant
364 increase in CD8 frequencies in the IngLNs but not in other tissues), indicating that the
365 observed differences, beyond being biologically robust and in agreement with the flow data,
366 were also statistically robust. Parametric tests were used in all analyses, with specific tests
367 indicated in the figure legends. All data is presented as bar graphs with mean ± SD. A p-value
368 <0.05 was considered to be statistically significant. ns = $p \geq 0.05$, * = $p<0.05$, **= $p<0.01$, *** =
369 $p<0.001$.

370 # Results
371
372 **Genetic GC block exacerbates autoimmune progression in a lupus model**
373 Chronic epicutaneous application of the synthetic, small-molecule TLR7 agonist, R848
374 (Resiquimod), has previously been demonstrated to induce a robust lupus-like autoimmune
375 phenotype in multiple genetic background strains of *Mus musculus* (Yokogawa et al., 2014).
376 Leveraging this model, we set out to investigate the relative importance of the extrafollicular
377 and GC pathways in the autoimmune response. To this end, we employed a transgenic Cre
378 driver line displaying expression of Cre under the Aicda promotor (Kwon et al., 2008). We
379 combined this with a conditional Bcl-6 knock-out line (Hollister et al., 2013), to achieve
380 deletion of Bcl-6 specifically in GC B cells. As Bcl-6 is a master transcriptional regulator of the
381 GC fates across GC B cells, T_{FH} cells and T_{FR} cells, this approach specifically prevents GC B cell
382 differentiation, without affecting Bcl-6 dependent T cell subsets essential to support both GC
383 and extrafollicular responses (Lee et al., 2011). As controls, we employed Cre negative Bcl-
384 $6^{flx/flx}$ littermates. In prior studies, when mice were treated with R848 3 times per week for 8
385 weeks, they displayed severe kidney damage, and 12 weeks of treatment led to a dramatic
386 degree of mortality (Yokogawa et al., 2014). As we wanted to investigate the importance of
387 pathways in production of autoantibodies and cell frequencies in the absence of secondary
388 effects caused by organ failure, we decided to treat mice 3 times weekly for only 4 weeks (**Fig.
389 1A**).
390
391 After 4 weeks of treatment, the Bcl-$6^{flx/flx}$ (Cre-) controls and the Aicda-Cre Bcl-$6^{flx/flx}$ (Cre+)
392 mice showed similar, significant increases in spleen weight upon R848 treatment (**Fig. 1B**).
393 Anti-dsDNA autoantibodies of the IgG2c subtype measured in serum were dramatically
394 elevated upon R848 treatment compared with untreated animals. Surprisingly, there was a
395 trend towards higher levels in treated Cre+ mice compared with treated Cre- mice (**Fig. 1C**).
396 A similar trend towards an increase was seen in total IgG2c levels (**Fig. 1D**). No statistically
397 significant differences in total IgG1 and total IgG3 levels were seen upon treatment (**Fig. 1E
398 and F**).
399
400 To validate the effect of R848 treatment and the integrity of the GC block in Cre+ mice, we
401 carried out immunofluorescence staining of spleens to identify GC formation (**Fig. 1G-J**). Using
402 the proliferation marker Ki67 and the naïve B cell marker IgD, it was evident that larger and
403 more frequent GCs were observed upon R848 treatment in Cre- animals (**Fig. 1G, H and K**).
404 Quantification revealed that this difference was statistically significant (**Fig. 1L**). Cre+ animals
405 did not display any baseline or R848-induced GCs (**Fig. 1I and J**). However, in Cre+ treated
406 mice we did observe many proliferating cells at the T-B border and in the red pulp, likely
407 abortive primary foci and extrafollicular foci, respectively.
408
409 Flow cytometric analyses of inguinal LNs (IngLNs), mesenteric LNs (MesLN), and the spleen
410 were carried out (**Fig. 1M-Q, Fig S1**). In treated animals, we saw slight increases in monocyte
411 and neutrophil frequencies in some of the tissues (**Fig. 1M and N**), and a slight increase in B
412 cell frequencies in the skin-draining IngLNs (**Fig. 1O**), which might be caused by the direct
413 stimulatory effect from the R848 treatment of the ear skin. We observed robust GC B cell
414 frequencies in Cre- R848 treated mice, compared to untreated littermates (**Fig. 1P**). No GC B
415 cells were found in Cre+ animals, further validating the fidelity of the GC block (**Fig. 1P**).
416 Surprisingly, despite this, we found a significant increase in PB and PC frequencies upon

417 treatment in both groups, and the level was significantly higher in the spleens of mice
418 harboring a GC block compared to Cre- R848-treated littermate controls (**Fig. 1Q**). This
419 observation corresponded well with the increase in plasma IgG2c autoantibody levels as well
420 as total IgG2c levels (**Fig 1C and D**). Taken together, this surprisingly indicated an exacerbated
421 autoimmune phenotype in GC block mice compared to GC sufficient mice upon R848
422 treatment.

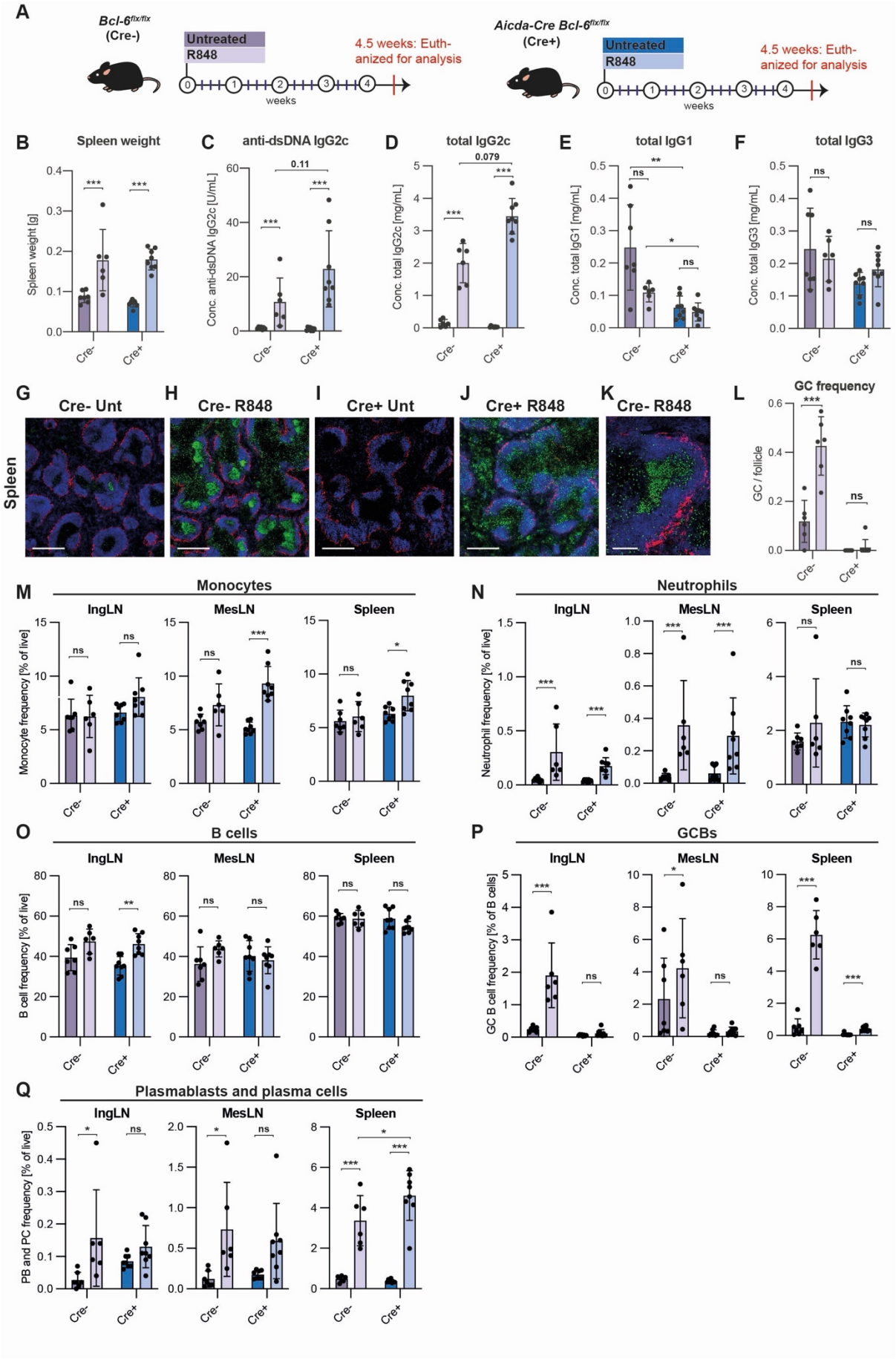
A
Bcl-6flx/flx
(Cre-)
Untreated
R848
4.5 weeks: Euth-anized for analysis
weeks
Aicda-Cre Bcl-6flx/flx
(Cre+)
Untreated
R848
4.5 weeks: Euth-anized for analysis
weeks
B Spleen weight
Spleen weight [g]
C anti-dsDNA IgG2c
Conc. anti-dsDNA IgG2c [U/mL]
D total IgG2c
Conc. total IgG2c [mg/mL]
E total IgG1
Conc. total IgG1 [mg/mL]
F total IgG3
Conc. total IgG3 [mg/mL]
Cre-
Cre+
G Cre- Unt
H Cre- R848
I Cre+ Unt
J Cre+ R848
K Cre- R848
Spleen
L GC frequency
GC / follicle
M Monocytes
IngLN
MesLN
Spleen
Monocyte frequency [% of live]
N Neutrophils
Neutrophil frequency [% of live]
O B cells
B cell frequency [% of live]
P GCBs
GC B cell frequency [% of B cells]
Q Plasmablasts and plasma cells
PB and PC frequency [% of live]

423

Figure 1. GC block causes increased levels of autoantibodies and PB/PCs in SLE-like mice. (**A**) Schematic overview of experimental setup and treatment protocol. Bcl-6$^{flx/flx}$ (Cre-, purple) and Aicda-Cre Bcl-6$^{flx/flx}$ (Cre+, blue) mice were either left untreated (dark color, n = 7 and n = 8, respectively) or treated with R848 (light color, n = 6 and n= 8, respectively), as indicated. (**B**) Spleen weights. (**C**) Anti-dsDNA IgG2c levels. (**D**) Total IgG2c levels. (**E**) Total IgG1 levels. (**F**) Total IgG3 levels. (**G**) Representative confocal micrograph of spleen from a Cre- untreated animal, stained for CD169 (red), IgD (blue) and Ki67 (green). Scale bar is 400 µm (**H**). As G, but for a Cre- R848-treated animal. (**I**) As G, but for a Cre+ untreated animal. (**J**) As G, but for a Cre+ R848-treated animal. (**K**) High-resolution image of a GC from a Cre- R848-treated mouse. Scale bar is 100 µm. **L**) GC per follicle in spleen. (**M**) Flow cytometry analyses of monocyte frequencies in IngLN, MesLN, and spleen (Ly6CG^{int} of live, singlet leukocytes). (**N**) As M, but neutrophil frequencies (Ly6CG^{hi} of live, singlet leukocytes). (**O**) As M, but B cell frequencies (B220^{+} CD4^{-} CD8^{-} of live, singlet leukocytes). (**P**) As M, but GCB frequencies (CD95^{hi} CD38^{lo} of B cells). (**Q**) As M, but PB and PC frequencies (CD138^{hi} of live, singlet leukocytes). Data are pooled from two independent experiments. Bar graphs show mean ± SD. Two-way ANOVA with Holm-Sidak's post hoc test was used to analyze the data. ns = p≥0.05, * = p<0.05, ** = p<0.01, *** = p<0.001.

To further understand the local effects of R848 treatment, we performed immunofluorescence microscopy analyses of draining auricular lymph nodes (AurLNs) from treated mice and untreated controls. We observed gross enlargement of the lymph nodes of treated animals, with a robust induction of GCs in Cre- R848-treated mice (**Fig. S2A**). In comparison, the Cre+ R848-treated mice had many proliferating cells outside the follicles (**Fig. S2A**). These dividing cells in the AurLNs overlapped to some extent with the PC marker CD138, pointing towards dividing extrafollicular PCs (**Fig. S2B**).

Nanoparticle tracking analyses

Using nanoparticle tracking analyses, we recently identified unique superoligomeric complexes (spMBL) formed between cell-free DNA and mannan-binding lectin (MBL), as a hallmark in blood samples from SLE patients and lupus mice (Juul-Madsen et al., 2021). These spMBL complexes correlated with disease activity in SLE patients, and correlated with formation of GCs and drove loss of immunological tolerance in a murine lupus model (564Igi). To further understand the importance of the increased anti-dsDNA IgG2c autoantibodies in Cre+ R848-treated mice, in the face of a complete absence of GCs, we implemented this nanoparticle tracking approach (**Fig. 2A-C**). We analyzed superoligomeric complexes in the band from 90-130 nm (**Fig. 2D and E**). In agreement with spMBL as a lupus marker, treated mice tended towards higher levels, as compared to untreated mice, but interestingly, we also observed a global trend towards higher levels in Cre+ compared to Cre- animals (**Fig. 2F**). Although they did not reach statistical significance, these observations were well in line with the previously noted increases in anti-dsDNA and total IgG2c antibodies upon R848 treatment, and in Cre+ compared to Cre- animals (**Fig. 1C**).

In our prior study on autoimmune mice carrying an autoreactive B cell receptor knock-in (564Igi) on a wild-type background (Juul-Madsen et al., 2021), a significant inverse correlation was found between the frequency of splenic GC B cells and the ratio between the spMBL and anti-dsDNA antibody concentrations measured in serum. This suggested that an excess of spMBL increased GC B cell formation while an excess of anti-dsDNA antibodies decreased GC B cell proliferation, or vice versa, indicating a potential negative feedback loop. In consideration of this, we next asked whether the same correlation could be established in the R848 model, and how this phenomenon was impacted in GC block mice.

472
473 In Cre- treated mice, GC B cell frequencies were positively correlated with the concentration
474 of spMBL particles in serum (**Fig. 2G**). Total IgG2c levels were similar between treated Cre+
475 and Cre- mice (**Fig. 2H**) with a significant positive correlation between anti-dsDNA IgG2c and
476 the level of spMBL particles (**Fig. 2I**). A significant positive correlation was also observed
477 between the frequency of splenic GC B cells and the ratio between the spMBL and total IgG2c
478 levels in serum (**Fig. 2J**). Conversely, a significant inverse correlation was found between the
479 frequency of splenic GC B cells and the ratio between the spMBL and anti-dsDNA IgG2c
480 antibody concentrations measured in serum (**Fig. 2K**). Taken together, these findings now
481 took our original observations from the autoreactive B cell receptor knock-in model (564Igi)
482 into the epicutaneous R848 model on wild-type (Cre-) background. Importantly, in Cre+ mice,
483 there was an uncoupling of the concentration of spMBL particles and GC B cell levels,
484 indicating that the GC block failed to curb the production of spMBL complexes.

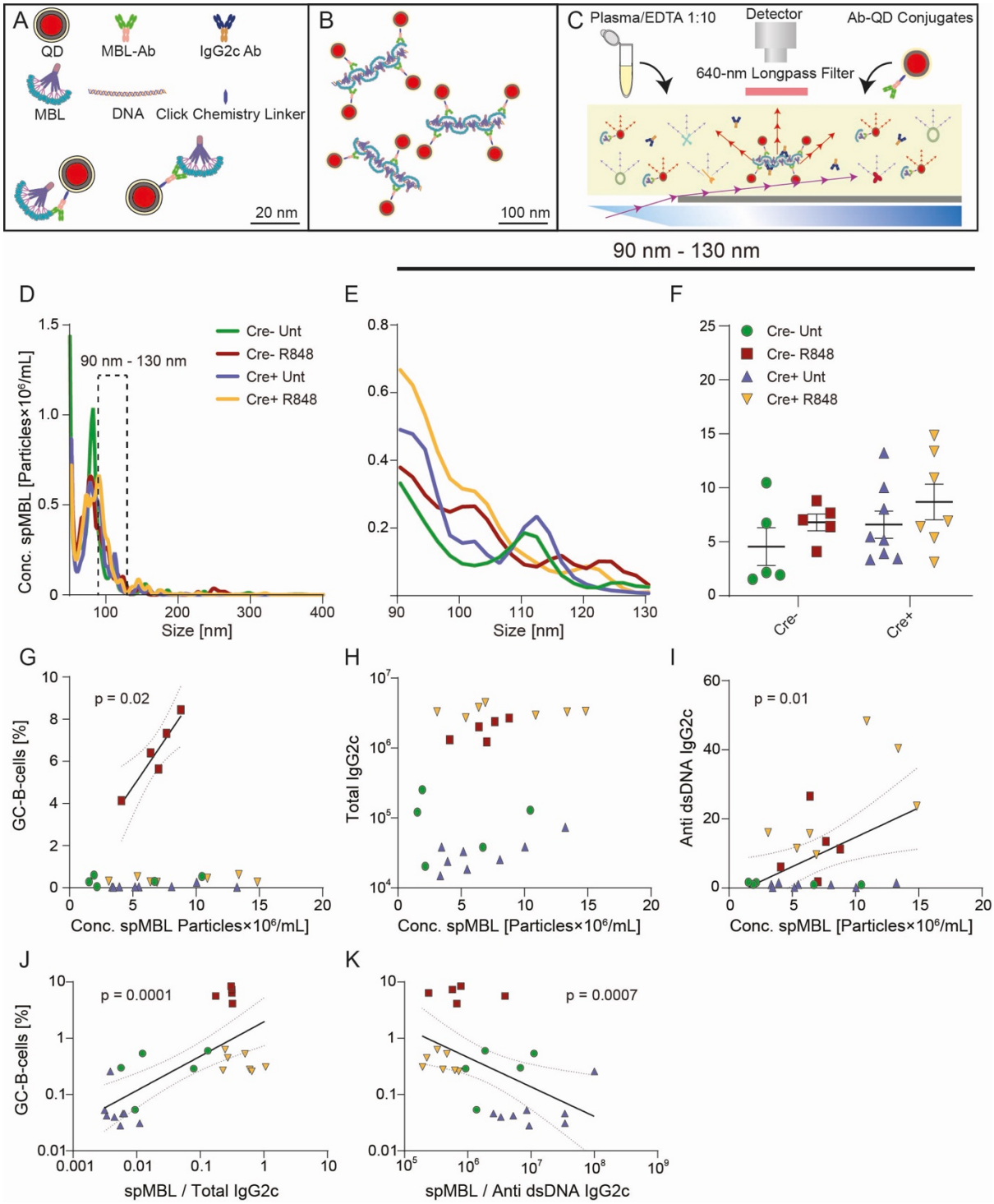

Figure 2. Trend towards increased levels of spMBL particles in serum from Cre+ R848 treated mice, and GC and autoantibody correlations with spMBL. (**A-C**) Schematic overview of experimental setup for spMBL analysis of serum samples. (**D**) Samples were tested for the size interval 90-130 nm from Aicda-Cre Bcl-6$^{flx/flx}$ (Untreated: blue, R848-treated: yellow) and Bcl-6$^{flx/flx}$ littermate controls (Untreated: green, R848-treated: red). (**E**) Zoom onto the range of 90 to 130 nm. (**F**) Graph showing measurements across treatment protocols for Cre- untreated (n= 5), Cre- R848-treated (n=5), Cre+ untreated (n=8), and Cre+ R848-treated (n=7) mice. (**G**) Correlation analysis of GCB vs. Conc. spMBL. (**H**) Correlation analysis of total IgG2c levels vs. Conc. spMBL. (**I**) Correlation analysis of anti-dsDNA IgG2c vs. Conc. spMBL. (**J**) Correlation analysis of GCB cells vs. spMBL/total IgG2c (**K**) Correlation analysis of GCB vs. spMBL/anti-dsDNA IgG2c. Two-way ANOVA with Holm-Sidak's post hoc test was

497 used to analyze the data in F. Linear regression models were used to analyze G-K. ns = p≥0.05, * =
498 p<0.05, ** = p<0.01, *** = p<0.001.
499
500
501 **Enhanced immune complex deposition in kidneys of R848-treated mice**
502 To understand the pathological importance of the GC block in R848-treated mice and the
503 elevated serum IgG2c, serum anti-dsDNA IgG2c and spMBL levels, we investigated whether
504 there were any pathological changes associated with lupus nephritis in the kidneys. First, we
505 carried out Periodic acid-Schiff (PAS) staining, which displayed no obvious kidney injury upon
506 R848 treatment (**Fig. 3A**). Apart from the presence of mesangial and capillary immune
507 deposits, histopathological changes associated with lupus nephritis may include increased
508 matrix or mesangial cellularity, endocapillary proliferation, thickening of capillary walls,
509 glomerular tuft necrosis, extracapillary proliferation (crescents), karyorrhexis, hyaline
510 thrombi (micronodular intracapillary aggregation of immune complexes), and glomerular
511 sclerosis (segmental or global), as well as, rarely, pathognomonic hematoxylin bodies
512 (Gasparotto et al., 2020; Weening et al., 2004). However, no significant histopathologic
513 findings were identified by light microscopy in any of the mice included in any of the groups.
514 In line with the PAS stainings, we did not observe any differences in glomerular nephrin levels
515 among the groups, suggesting normal glomerular podocytes (**Fig. 3B**). As we could not identify
516 any gross pathological changes nor changes in nephrin levels in the kidneys upon treatment,
517 this verified our short-term treatment strategy in terms of the goal to investigate early
518 immune-driven events in the absence of any secondary pathology.
519
520 To evaluate if immune complex deposition occurred in the kidney glomeruli, and if there were
521 any differences between GC-sufficient and deficient groups, we performed
522 immunofluorescence staining of kidney sections targeting total Ig, C3, and IgG2c (**Fig 3B, 3C,**
523 **3E-G**). The total Ig levels in glomeruli were clearly increased upon R848-treatment.
524 Interestingly, we found a trend towards an increase in the total Ig levels of Cre+ mice
525 compared with littermate R848-treated controls (**Fig. 3B and E**). We also found that there was
526 a significant increase of antibodies of the pathogenic subtype IgG2c upon R848 treatment
527 (**Fig. 3C and G**), and a trend towards an increase in C3 deposition upon R848-treatment (**Fig.**
528 **3C and F**). However, differences between Cre+ and Cre- R848-treated groups were seen
529 neither in C3 nor IgG2c levels (**Fig. 3F and G**).
530
531 Taken together, R848-treated mice displayed immune complex deposition in glomeruli, based
532 on an increased level of C3, total Ig and IgG2c (**Fig. 3E-G**). We corroborated these findings by
533 peroxidase-stainings, as a corollary to the immunofluorescence microscopy, and this
534 confirmed the glomerular changes in total Ig, C3 and IgG2c upon R848-treatment (**Fig S3**).
535 Based on the immunofluorescence and immunoperoxidase findings of immune complex
536 deposition (Ig, IgG2c and C3), in the absence of gross histopathological changes of the kidneys,
537 this corresponds to Class I pathology (minimal mesangial lupus nephritis) displaying mesangial
538 immune deposits without mesangial hypercellularity, as defined by the International Society
539 of Nephrology (ISN) and the Renal Pathology Society (RPS) 2004 classification system
540 (Weening et al., 2004).

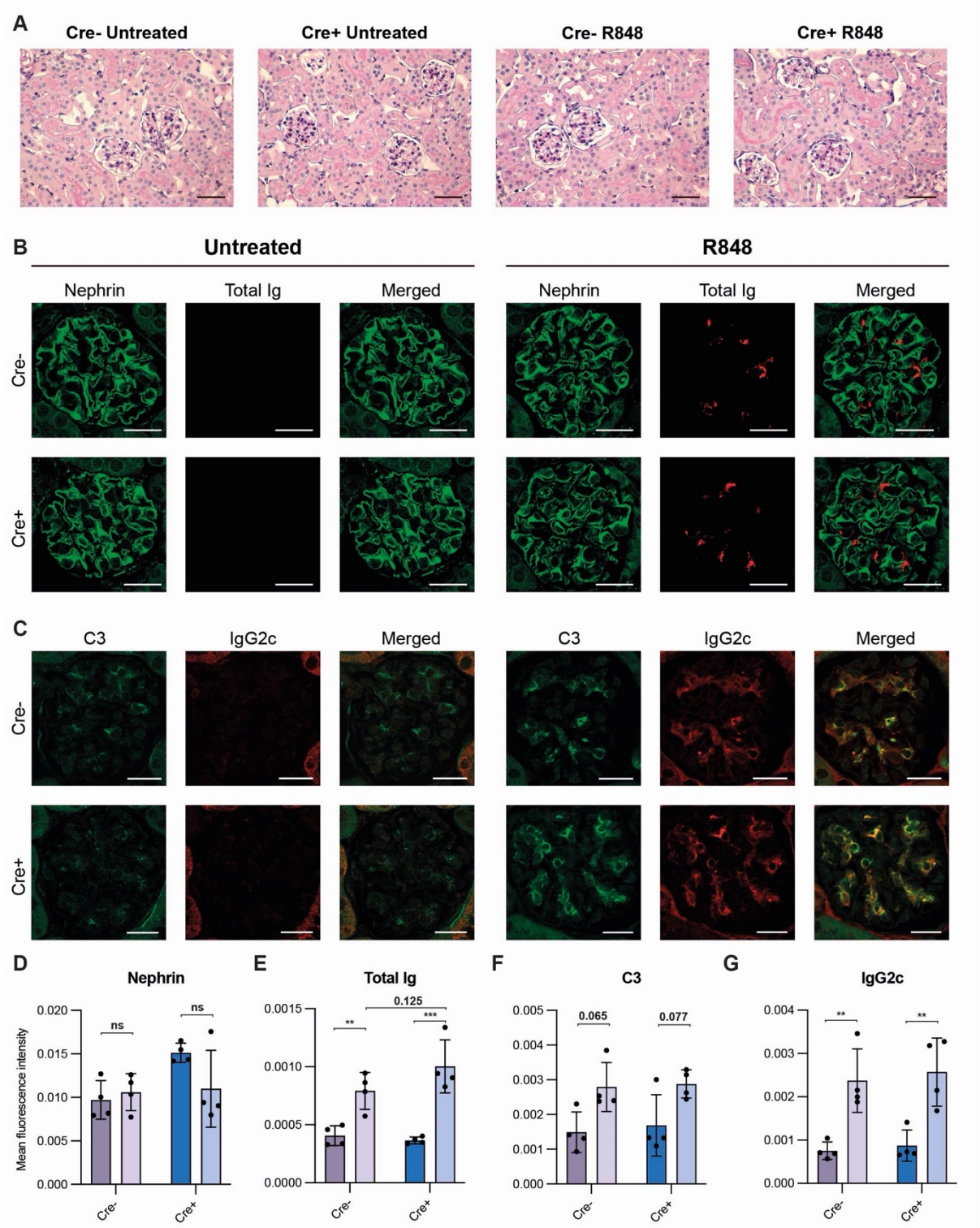

Figure 3. Kidney staining reveal immune complex deposition in R848-treated mice. (**A**) PAS stained kidney sections of Cre- untreated (n=4), Cre- R848-treated (n=4), Cre+ untreated (n=4), Cre+ R848-treated (n=4). Scale bar is 50 µm. (**B**) Immunofluorescence staining of kidney sections targeting nephrin (green) and total Ig (red). (**C**) Immunofluorescence staining of kidney sections targeting C3 (green) and IgG2c (red). (**D**) Quantification of immunofluorescence staining targeting nephrin, (**E**) total Ig, (**F**) C3, (**G**) and IgG2c. Scale bar is 20 µm. Two-way ANOVA with Holm-Sidak's post hoc test was used to analyze the data. Bars show mean ± SD. ns = p>0.05, * = p < 0.05, **= p<0.01, *** = p < 0.001.

551 **An intrinsic GC block drives B cell differentiation into terminally differentiated PCs**
552 To investigate whether a B cell intrinsic block of the GC pathway affects their capacity to
553 differentiate into PBs and PCs, we leveraged a modified *in vitro* setup for induced GC B cell
554 (iGB) cultures (Kuraoka et al., 2016; Nojima et al., 2011) (**Fig. 4A**). Naïve B cells purified from
555 Cre- and Cre+ Bcl-6$^{flx/flx}$ mice by negative magnetic-activated cell sorting were seeded onto
556 fibroblast feeder cells expressing CD40L, IL-21 and BAFF, and stimulated with IL-4 (**Fig. 4A**).
557
558 The combination of CD40L, BAFF, IL-21, and IL-4 stimulation has previously been shown to
559 induce a robust expansion of B cells with a GC-like phenotype, followed by differentiation of
560 the cells into PBs and finally PCs (Kuraoka et al., 2016; Nojima et al., 2011). Following
561 stimulation of cultures with IL-4, we performed flow cytometric analyses and observed
562 significantly higher B cell (B220+, CD138neg) frequencies in cultures derived from Cre- mice,
563 compared to those derived from Cre+ mice (**Fig. 4B and E**). This was mirrored by a similar
564 relative increase in PBs (B220+, CD138+) in Cre- cultures (**Fig. 4B and D**), but a relative
565 decrease in PCs (B220neg, CD138+) (**Fig. 4B and C**). Of interest, the total number of cells in
566 the live gate for Cre- cultures was approximately 4 times higher than that of Cre+ cultures
567 (Cre-: 140,000 vs. Cre+: 33,000, **Fig. S4C**). To understand this difference in cell numbers, we
568 investigated whether the Cre+, and hence Bcl-6 deficient, B cells had an increased propensity
569 to undergo apoptosis, because Bcl-6 has previously been reported to suppress P53 and inhibit
570 apoptosis in GC B cells (Phan & Dalla-Favera, 2004). Somewhat surprisingly, we found that
571 upon IL-4 stimulation, there was no difference in the frequency of dead cells (**Fig. 4F and G**),
572 a slight and significant drop in apoptotic cell frequency (**Fig. 4F and H**), and a corresponding
573 increased relative frequency of live cells in Cre+ cultures compared to Cre- cultures on day 6
574 (**Fig. 4F and I**). However, at day 10 there were no significant differences in live, apoptotic, nor
575 necrotic cell frequencies between Cre- and Cre+ cultures (**Fig. 4J-M**). Thus, apoptosis could
576 not account for the dramatic difference in resulting cell numbers between Cre+ and Cre- (**Fig.
577 S4C**). Taken together, this suggested that the higher overall cell numbers in Cre- cultures was
578 not simply a reflection of increased apoptosis among Bcl-6 deficient cells in Cre+ cultures, but
579 rather represented an improved intrinsic proliferative potential of the Bcl-6 sufficient cells.
580
581 In summary, our iGB experiments revealed a vigorous expansion of B cells and PCs in Cre-
582 cultures, but less pronounced PC differentiation, whereas Cre+ cultures conversely displayed
583 a lesser degree of proliferation but more pronounced PC differentiation. This suggested that
584 B cells with an intrinsic GC block may differentiate quicker to PCs, and thereby lose their
585 proliferative capacity, a notion that is in line with the established function of Bcl-6 in
586 repressing upregulation of Blimp-1 (Vasanwala et al., 2002).

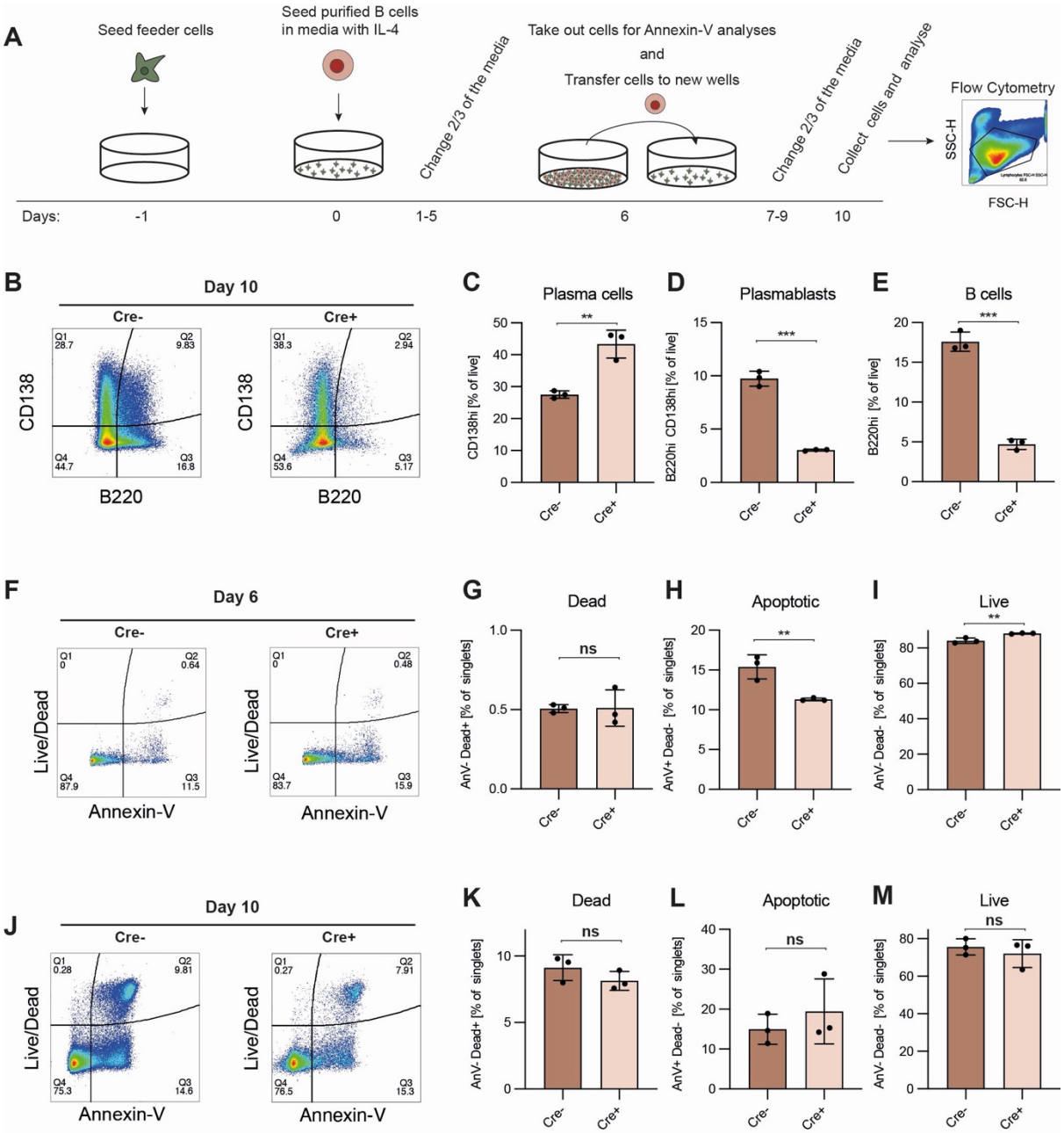

Figure 4. Bcl-6 deficient cells more readily differentiate into PCs in iGB cultures. B cells in iGB cultures were treated with IL-4 in conjunction with CD40L, BAFF, and IL-21. (**A**) Schematic overview of the iGB culture system. (**B**) Representative terminal CD138 vs. B220 bivariate plot for iGB cultured B cells stimulated with IL-4. (**C**) Bar graph showing B cell frequencies (B220+, CD138neg). (**D**) As C, but showing PB frequencies (B220+, CD138+). (**E**) As for C, but showing PC frequencies (B220neg, CD138+). Data are representative of three independent experiments with a cumulative 8 replicates in total. Bar graphs show mean ± SD. (**F**) Day 6 representative terminal Live/Dead vs. Annexin V bivariate plot for iGB cultured B cells stimulated with IL-4. (**G**) Bar graph showing dead cell frequencies (AnV-, Dead+). (**H**) As F, but showing apoptotic cell frequencies (AnV+, Dead-). (**I**) As for F, but showing live cell frequencies (AnV-, Dead-). (**J**) Day 10 representative terminal Live/Dead vs. Annexin V bivariate plot for iGB cultured B cells stimulated with IL-4. (**K**) Bar graph showing dead cell frequencies (AnV-, Dead+). (**L**) As for K, but showing apoptotic cell frequencies (AnV+, Dead-). (**M**) As for K, but showing live cell frequencies (AnV-, Dead-). Data for apoptosis assays are from one experiment with 3 replicates. Bar graphs show mean ± SD. Unpaired t-tests were used to analyze all datasets. ns = p≥0.05, * = p<0.05, ** = p<0.01, *** = p<0.001.

603
604 **B cells harboring a GC block competitively contribute to the PC compartment in an**
605 **autoreactive setting**
606 Our observation that Bcl-6 deficient B cells rapidly lost their replicative potential *in vitro* (**Fig.**
607 **4**) was somewhat at odds with our *in vivo* observations from the R848 model, which displayed
608 a global increase in PCs and autoantibodies (**Fig. 1**). This is because even if Bcl-6 deficient cells
609 more readily became PCs, their poorer capacity to expand compared to Bcl-6 sufficient cells
610 would be predicted to limit PC output. However, it was possible that the constant
611 autoinflammatory drive in an *in vivo* setting where B cells were globally prevented from
612 differentiating down the GC pathway would dysregulate the PC differentiation process and
613 disproportionately drive extrafollicular differentiation. To address this possibility, we asked
614 whether B cells with a GC block would be precluded from contributing to the PC pool in an
615 environment where a large fraction of competitor B cells could form GCs. To achieve this, we
616 leveraged a mixed bone-marrow chimera model allowing interrogation of the competitive
617 potential of B cells with a defined genetic defect in a lupus-like setting (Degn, van der Poel,
618 Firl, et al., 2017; Wittenborn et al., 2021). In this model, an autoreactive B cell receptor knock-
619 in clone (clone 564Igi) initiates an autoreactive process that subsequently recruits proto-
620 autoreactive B cells from the non-564Igi B cell population. The B cells derived from the 564Igi
621 compartment eventually are outcompeted and constitute only a minor fraction of the total B
622 cell repertoire. Uniquely to this model, the spontaneous autoreactive GCs established by the
623 564Igi compartment become populated and chronically self-sustained by the non-564Igi (WT)
624 B cells and gain independence from the initial 564Igi trigger. From around six weeks after
625 reconstitution, GCs are almost exclusively (~95%) composed of WT-derived cells (Degn, van
626 der Poel, Firl, et al., 2017; Green et al., 2021). Reconstitution with a third of each of 564Igi
627 BM, BM from a wild-type donor, and BM from a donor harboring a specified genetic defect,
628 hence results in chimeras with two equal-sized compartments of B cells sufficient or deficient
629 in the gene of interest. With the use of appropriate congenic markers, their competitive
630 recruitment and participation in the autoreactive GC reaction and relative contribution to the
631 PC compartment can subsequently be evaluated to elucidate the functional relevance of their
632 intrinsic molecular differences. Accordingly, we set up mixed BM chimeras by irradiating WT
633 CD45.1/1 recipients and reconstituting with 1/3 of each of 564Igi knock-in BM, WT CD45.1/1
634 BM, and either Aicda-Cre+ Bcl-6$^{flx/flx}$ or Aicda-Cre- Bcl-6$^{flx/flx}$ BM (**Fig. 5A and S5**).
635
636 There were no differences in the basic parameters when comparing Cre- control BM chimera
637 mice with Cre+ BM chimera mice, in which approximately 50% of the B cells harbored a GC
638 block (**Fig. 5B-H**). That is, aside from a very small but significant relative increase of CD8 T cells
639 in IngLN of Cre+ chimeras, we saw no statistically significant differences in anti-dsDNA IgG2c
640 (**Fig. 5B**), total anti-dsDNA Ig (**Fig. 5C**), B cell frequencies (**Fig. 5D**), CD4 and CD8 T cell
641 frequencies (**Fig. 5E and F, respectively**), overall GC B cell frequencies (**Fig. 5G**) and PB/PC
642 frequencies (**Fig. 5H**) between the groups. This confirmed that the two groups of chimeras
643 were comparable and had robust GCB and PC compartments. In the total B cell compartment,
644 CD45.2 positive cells were present at levels comparable to that of CD45.1 cells in both Cre-
645 (**Fig. 5I**) and Cre+ (**Fig. 5J**) chimeras. However, within the GC B cell gate, CD45.2 cells were
646 robustly represented in Cre- chimeras, but virtually absent in Cre+ chimeras (**Fig. 5I and J**).
647 When quantifying this effect across chimeras and expressing as the ratio of CD45.2 of GCB
648 relative to CD45.2 of total B cells, it was clear that Bcl-6 deficient cells, as expected from their
649 genetic deficiency, were incapable of contributing to the GC compartment (**Fig. 5K**). However,

650 when similarly comparing PB/PC ratio over B cells, the cells harboring a GC block remained
651 able to contribute to the final PB/PC pool, albeit underrepresented relative to the competitor
652 cells (**Fig. 5L**). Taken together, these findings demonstrated that in a GC-sufficient
653 environment, B cells experiencing a block in their ability to partake in the GC reaction readily
654 contributed to the PB and PC compartments.

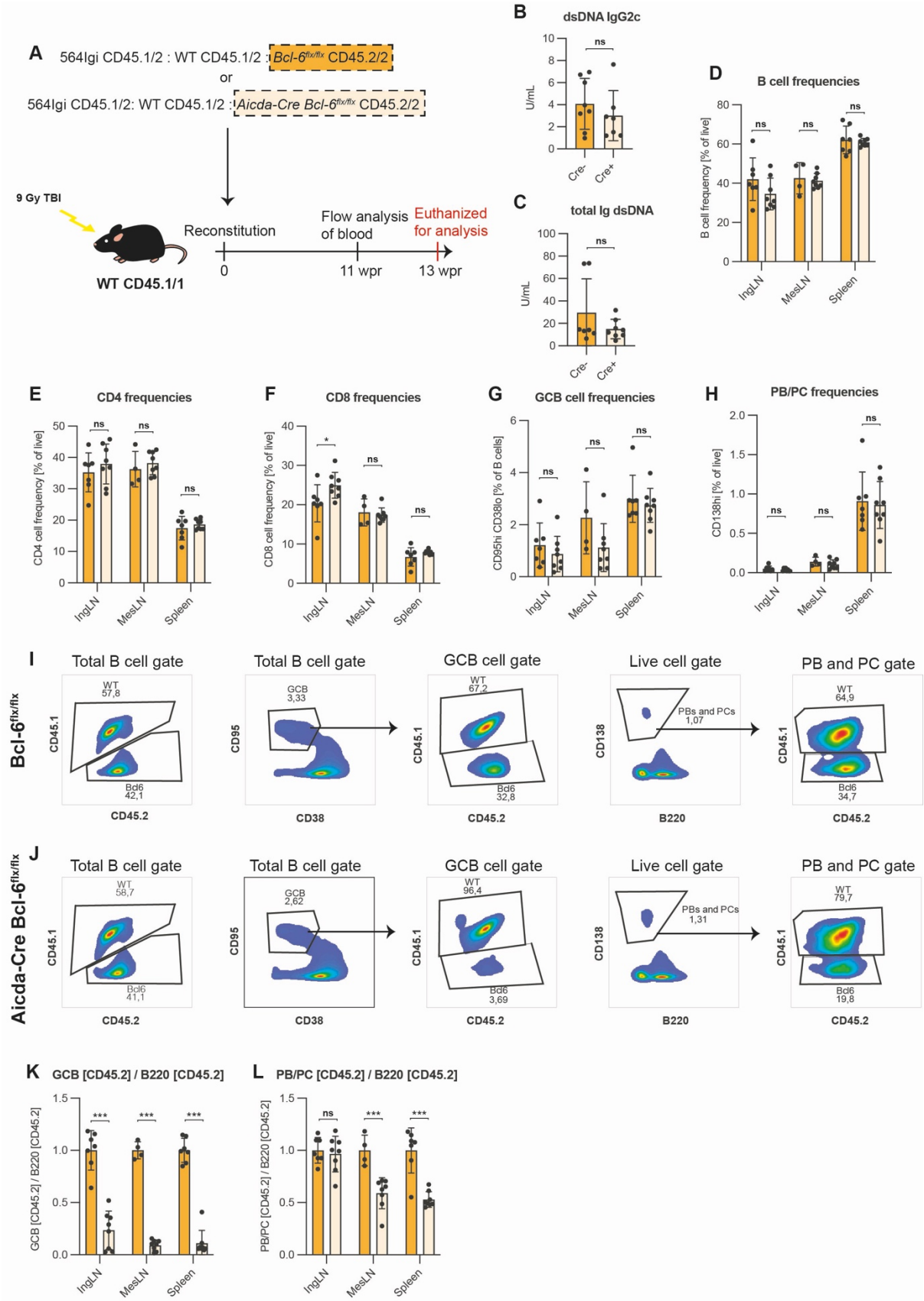

Figure 5. B cells harboring a GC block contribute to the PC lineage in a GC sufficient environment. (**A**) Schematic overview of the mixed bone-marrow chimera setup. Lethally irradiated CD45.1/1 recipients were reconstituted with CD45.2/2 564Igi BM, WT CD45.1/2 BM and either Bcl-6$^{flx/flx}$ (Cre-, orange, n =

660 7) or Aicda-Cre Bcl-6$^{flx/flx}$ (Cre+, light orange, n=8). (**B**) dsDNA IgG2c TRIFMA. (**C**) total Ig TRIFMA. (**D**)
661 Flow cytometric analysis of B cell frequencies (B220^{+} of live, singlets). (**E**) CD4 frequencies (CD4 of live,
662 singlets). (**F**) CD8 frequencies. (**G**) GCB frequencies (CD95^{hi} CD38^{lo} of B cells). (**H**) PB/PC frequencies
663 (CD138^{hi} of live, singlets). (**I**) Representative bivariate plots with gates for Bcl-6$^{flx/flx}$ chimeras. (**J**)
664 Representative bivariate plots with gates for Aicda-Cre Bcl-6$^{flx/flx}$ chimeras. (**K**) Ratio of CD45.2+ of GCB
665 to CD45.2+ of total B cells. (**L**) Ratio of CD45.2+ of PBs/PCs to CD45.2+ of total B cells. The results are
666 obtained from a single experiment with the number of mice given above. Bar graphs show mean $\pm$
667 SD. ns = $p \geq 0.05$, * = $p<0.05$, **= $p<0.01$, *** = $p<0.001$.

668 # Discussion

669 GCs are believed to be the nexus of autoreactive responses in a range of autoimmune
670 diseases. Due to their role in potent antibody responses, memory generation, and long-lived
671 PC formation, there has been extensive interest in targeting GCs in autoimmune disease. The
672 strategy has proven useful in autoimmune models, but due to off-target effects, did not
673 initially progress through clinical trials (Degn, van der Poel, & Carroll, 2017; Karnell et al.,
674 2019). Considerable efforts have, however, been aimed at circumventing the off-target
675 effects to bring this strategy to market (Espie et al., 2020; Karnell et al., 2019). This
676 notwithstanding, a recent study reported that extrafollicular B cell differentiation into short-
677 lived antibody-forming cells is a key mechanism of anti-DNA autoreactivity (Soni et al., 2020),
678 and it has been argued that more attention should be paid to the non-GC responses, as these
679 may play a critical role in humoral immunity in both mice and men (Jenks et al., 2019).
680
681 Here, we took an unbiased approach and asked to what extent a specific genetic block of GCs
682 would ameliorate autoreactive manifestations in a lupus-like disease model. To our surprise,
683 we found blocking GCs did not lessen autoreactive manifestations, but in some cases
684 worsened these. Upon autoimmune induction, we observed a trend towards an increase in
685 anti-dsDNA antibodies of the IgG2c isotype (**Fig. 1C**) and total IgG2c antibody (**Fig. 1D**) in GC
686 block mice, compared to WT. These changes were also mirrored by a significantly higher
687 frequency of PB/PCs in the spleens of GC block mice, despite a total absence of GCs. In
688 agreement with this, we observed robust deposition of immune complexes in the kidney
689 glomeruli of GC block mice, at least on par with that of GC sufficient controls (**Fig. 3**). This
690 indicated that the extrafollicular pathway could compensate, and in some cases even
691 augment, the autoreactive response.
692
693 To understand the B cell intrinsic effect of a GC block, we leveraged an induced GC B cell
694 culture system. It has previously been noted that Bcl-6 expression can inhibit apoptosis in
695 numerous cell types including (GC) B cells (Kumagai et al., 1999; Kurosu et al., 2003; Phan &
696 Dalla-Favera, 2004). Yet, contrary to expectations, GC block B cells did not display a
697 significantly increased propensity to undergo apoptosis (**Fig. 4H and L**), rather, they much
698 more readily underwent terminal differentiation to PCs, and had a dramatically reduced
699 capacity to expand compared to their wild type counterparts (**Fig. 4**). However, this agreed
700 well with the established cross-regulation between Bcl-6 and Blimp-1, the master regulator
701 of the PC fate, also known as Prdm1 (Vasanwala et al., 2002). Although the increased
702 propensity for terminal PC differentiation was, in principle, well in line with our *in vivo*
703 observations, the lack of proliferative capacity was at the same time at odds with the dramatic
704 PC output in the mice harboring a GC block in B cells. This suggested that the PC differentiation
705 process in mice displaying a global GC block in B cells might be dysregulated, potentially as a
706 consequence of absence of GC-derived antibody feedback, as previously suggested for GC B
707 cells (Zhang et al., 2013). To address this possibility, we asked whether B cells with a GC block
708 would be precluded from contributing to the PC pool in a GC sufficient environment. Our
709 findings demonstrated that this was not the case, although the relative contribution of GC
710 block B cells to the PC pool was smaller than that of GC sufficient B cells (**Fig. 5**). However,
711 given their inability to expand in GCs, the magnitude of the contribution of GC block B cells to
712 the PC compartment in direct competition with GC-sufficient B cells was remarkable. In the
713 infectious setting, an early wave of extrafollicular PCs is crucial for the initial antibody
714 response. However, most PCs produced by the extrafollicular response undergo apoptosis

715 within a matter of days, and the global response becomes dominated by GC-derived
716 responses. In the chronic autoreactive setting, however, the continuous fueling of the
717 autoimmune process may continually renew this population.
718
719 We may speculate that the somewhat lower contribution of the extrafollicular PC
720 compartment in the mixed chimera model compared to that of the R848 model could be a
721 consequence of the markedly different time scales of the two experiments: the mixed
722 chimeras were analyzed 13 weeks post reconstitution, whereas the R848 mice were analyzed
723 4.5 weeks after commencement of treatment. This could be important, because at this point
724 it remains unclear whether the GC responses observed in our models contribute a
725 qualitatively different response to the autoimmune progression, e.g., through production of
726 memory B cells and long-lived PCs that may perpetuate and dominate the chronic response
727 over longer periods of time. By extension, the GC pathway may differentially allow epitope
728 spreading and inclusion of alternative antigens over time, as seen in human SLE patients
729 (Arbuckle et al., 2003). At least, it seems plausible that the longer the autoimmune process
730 has persisted, the more the long-lived GC responses and their derived memory output come
731 to dominate the process. However, conversely, the short-lived extrafollicular responses may
732 govern the early stages of the response and, as previously suggested, the very early break-of-
733 tolerance driven by nucleic acid-containing antigens (Soni et al., 2020; Sweet et al., 2011).
734
735 Interestingly, due to its more potent nature, The GC reaction is also believed to be subject to
736 a much higher level of control, through a continued requirement for linked recognition in
737 successive rounds of diversity generation. Furthermore, a specialized subset of Tregs, T_{FR}s,
738 exert a dominant negative level of control on the GC reaction (Fahlquist Hagert & Degn, 2020).
739 Hence it may be that the extrafollicular pathway in essence represents an evolutionary
740 'backdoor to autoimmunity', unguarded due to its relative insignificance in terms of high-
741 quality, affinity-matured, and memory-inducing antibody responses. In this context, it is
742 fortunate that current CD40L targeting strategies block both the GC and extrafollicular
743 response. However, we suggest that future efforts should be aimed at further elucidating the
744 relative contributions of the extrafollicular and GC pathways. We may speculate that specific
745 targeting of the extrafollicular pathway would be a superior strategy, as it would
746 preferentially block the low quality and poorly controlled responses driving autoimmune
747 progression, while leaving intact the more stringently controlled and high-quality responses
748 that provide protection against infectious agents. Unfortunately, there is much more limited
749 knowledge regarding the biology of the extrafollicular responses, and no transgenic or
750 pharmacologic strategy allowing specific blockade of this pathway exists, making it difficult to
751 evaluate in animal models.
752
753 In summary, our findings here demonstrate that a complete or partial block of the GC
754 pathway is insufficient to curb autoreactive PC differentiation and might in some instances in
755 fact exacerbate the autoimmune progression. The GC commitment is controlled by the
756 expression level of the master transcriptional repressor, Bcl-6 (Robinson et al., 2020), which
757 regulates the GC fates across GC B cells, T_{FH} cells and T_{FR} cells. Interestingly, in the context of
758 the COVID-19 pandemic, it has been observed that Bcl-6^+ GC B cells and Bcl-6^+ T_{FH} cells are
759 markedly diminished in SARS-CoV-2 infection (Kaneko et al., 2020). It has also been found that
760 critically ill SARS-CoV-2 patients display hallmarks of extrafollicular B cell activation and
761 shared B cell repertoire features previously described in autoimmune settings (Knight et al.,

2021; Woodruff et al., 2020). This further highlights the potential link between aberrant extrafollicular responses and autoimmune manifestations.

Conflict of Interest statement

TV-J and KJ-M are inventors on a submitted patent application (PCT/EP2020/082837), owned by Aarhus University, related to human spMBL as a biomarker for SLE. All other authors declare that the research was conducted in the absence of any commercial or financial relationships that could be construed as a potential conflict of interest.

Acknowledgements

We thank Hanne Sidelmann for her contributions to immunofluorescence and immunohistochemical staining of kidneys. We would like to acknowledge the AU FACS Core facility for their support and feedback on data related to flow cytometry. We also thank the BioImaging Core at Health for support with microscopy.

Funding

This project was funded by the Novo Nordisk Foundation (NNF19OC0058454) and the Independent Research Fund Denmark through a *Sapere Aude* Research Leader grant to SED (9060-00038B).

References

Akkaya, M., Akkaya, B., Kim, A. S., Miozzo, P., Sohn, H., Pena, M., Roesler, A. S., Theall, B. P., Henke, T., Kabat, J., Lu, J., Dorward, D. W., Dahlstrom, E., Skinner, J., Miller, L. H., & Pierce, S. K. (2018). Toll-like receptor 9 antagonizes antibody affinity maturation. *Nat Immunol*, *19*(3), 255-266. https://doi.org/10.1038/s41590-018-0052-z

Arbuckle, M. R., McClain, M. T., Rubertone, M. V., Scofield, R. H., Dennis, G. J., James, J. A., & Harley, J. B. (2003). Development of autoantibodies before the clinical onset of systemic lupus erythematosus. *N Engl J Med*, *349*(16), 1526-1533. https://doi.org/10.1056/NEJMoa021933

Berland, R., Fernandez, L., Kari, E., Han, J. H., Lomakin, I., Akira, S., Wortis, H. H., Kearney, J. F., Ucci, A. A., & Imanishi-Kari, T. (2006). Toll-like receptor 7-dependent loss of B cell tolerance in pathogenic autoantibody knockin mice. *Immunity*, *25*(3), 429-440. https://doi.org/10.1016/j.immuni.2006.07.014

Cornaby, C., Gibbons, L., Mayhew, V., Sloan, C. S., Welling, A., & Poole, B. D. (2015). B cell epitope spreading: mechanisms and contribution to autoimmune diseases. *Immunol Lett*, *163*(1), 56-68. https://doi.org/10.1016/j.imlet.2014.11.001

Degn, S. E., van der Poel, C. E., & Carroll, M. C. (2017). Targeting autoreactive germinal centers to curb autoimmunity. *Oncotarget*, *8*(53), 90624-90625. https://doi.org/10.18632/oncotarget.21701

Degn, S. E., van der Poel, C. E., Firl, D. J., Ayoglu, B., Al Qureshah, F. A., Bajic, G., Mesin, L., Reynaud, C. A., Weill, J. C., Utz, P. J., Victora, G. D., & Carroll, M. C. (2017). Clonal Evolution of Autoreactive Germinal Centers. *Cell*, *170*(5), 913-926 e919. https://doi.org/10.1016/j.cell.2017.07.026

Domeier, P. P., Schell, S. L., & Rahman, Z. S. (2017). Spontaneous germinal centers and autoimmunity. *Autoimmunity*, *50*(1), 4-18. https://doi.org/10.1080/08916934.2017.1280671

Elsner, R. A., & Shlomchik, M. J. (2020). Germinal Center and Extrafollicular B Cell Responses in Vaccination, Immunity, and Autoimmunity. *Immunity*, *53*(6), 1136-1150. https://doi.org/10.1016/j.immuni.2020.11.006

Espie, P., He, Y., Koo, P., Sickert, D., Dupuy, C., Chokote, E., Schuler, R., Mergentaler, H., Ristov, J., Milojevic, J., Verles, A., Groenewegen, A., Auger, A., Avrameas, A., Rotte, M., Colin, L., Tomek, C. S., Hernandez-Illas, M., Rush, J. S., & Gergely, P. (2020). First-in-human clinical trial to assess pharmacokinetics, pharmacodynamics, safety, and tolerability of iscalimab, an anti-CD40 monoclonal antibody. *Am J Transplant*, *20*(2), 463-473. https://doi.org/10.1111/ajt.15661

Fahlquist Hagert, C., & Degn, S. E. (2020). T follicular regulatory cells: Guardians of the germinal centre? *Scand J Immunol*, *92*(4), e12942. https://doi.org/10.1111/sji.12942

Gasparotto, M., Gatto, M., Binda, V., Doria, A., & Moroni, G. (2020). Lupus nephritis: clinical presentations and outcomes in the 21st century. *Rheumatology (Oxford)*, *59*(Suppl5), v39-v51. https://doi.org/10.1093/rheumatology/keaa381

Green, K., Wittenborn, T. R., Fahlquist-Hagert, C., Terczynska-Dyla, E., van Campen, N., Jensen, L., Reinert, L., Hartmann, R., Paludan, S. R., & Degn, S. E. (2021). B Cell Intrinsic STING Signaling Is Not Required for Autoreactive Germinal Center Participation [Original Research]. *Frontiers in Immunology*, *12*(5184). https://doi.org/10.3389/fimmu.2021.782558

Hollister, K., Kusam, S., Wu, H., Clegg, N., Mondal, A., Sawant, D. V., & Dent, A. L. (2013). Insights into the role of Bcl6 in follicular Th cells using a new conditional mutant mouse model. *J Immunol*, *191*(7), 3705-3711. https://doi.org/10.4049/jimmunol.1300378

Jenks, S. A., Cashman, K. S., Woodruff, M. C., Lee, F. E., & Sanz, I. (2019). Extrafollicular responses in humans and SLE. *Immunol Rev*, *288*(1), 136-148. https://doi.org/10.1111/imr.12741

Juul-Madsen, K., Troldborg, A., Wittenborn, T. R., Axelsen, M. G., Zhao, H., Klausen, L. H., Luecke, S., Paludan, S. R., Stengaard-Pedersen, K., Dong, M., Moller, H. J., Thiel, S., Jensen, H., Schuck, P., Sutherland, D. S., Degn, S. E., & Vorup-Jensen, T. (2021). Characterization of DNA-protein complexes by nanoparticle tracking analysis and their association with systemic lupus erythematosus. *Proc Natl Acad Sci U S A*, *118*(30). https://doi.org/10.1073/pnas.2106647118

Kaneko, N., Kuo, H. H., Boucau, J., Farmer, J. R., Allard-Chamard, H., Mahajan, V. S., Piechocka-Trocha, A., Lefteri, K., Osborn, M., Bals, J., Bartsch, Y. C., Bonheur, N., Caradonna, T. M., Chevalier, J., Chowdhury, F., Diefenbach, T. J., Einkauf, K., Fallon, J., Feldman, J., . . . Massachusetts Consortium on Pathogen Readiness Specimen Working, G. (2020). Loss of Bcl-6-Expressing T Follicular Helper Cells and Germinal Centers in COVID-19. *Cell*, *183*(1), 143-157 e113. https://doi.org/10.1016/j.cell.2020.08.025

Karnell, J. L., Albulescu, M., Drabic, S., Wang, L., Moate, R., Baca, M., Oganesyan, V., Gunsior, M., Thisted, T., Yan, L., Li, J., Xiong, X., Eck, S. C., de Los Reyes, M., Yusuf, I., Streicher, K., Muller-Ladner, U., Howe, D., Ettinger, R., . . . Drappa, J. (2019). A CD40L-targeting protein reduces autoantibodies and improves disease activity in patients with autoimmunity. *Sci Transl Med*, *11*(489). https://doi.org/10.1126/scitranslmed.aar6584

Knight, J. S., Caricchio, R., Casanova, J. L., Combes, A. J., Diamond, B., Fox, S. E., Hanauer, D. A., James, J. A., Kanthi, Y., Ladd, V., Mehta, P., Ring, A. M., Sanz, I., Selmi, C., Tracy, R. P., Utz, P. J., Wagner, C. A., Wang, J. Y., & McCune, W. J. (2021). The intersection of COVID-19 and autoimmunity. *J Clin Invest*, *131*(24). https://doi.org/10.1172/JCI154886

Kumagai, T., Miki, T., Kikuchi, M., Fukuda, T., Miyasaka, N., Kamiyama, R., & Hirosawa, S. (1999). The proto-oncogene Bc16 inhibits apoptotic cell death in differentiation-induced mouse myogenic cells. *Oncogene*, *18*(2), 467-475. https://doi.org/10.1038/sj.onc.1202306

Kuraoka, M., Schmidt, A. G., Nojima, T., Feng, F., Watanabe, A., Kitamura, D., Harrison, S. C., Kepler, T. B., & Kelsoe, G. (2016). Complex Antigens Drive Permissive Clonal Selection in Germinal Centers. *Immunity*, *44*(3), 542-552. https://doi.org/10.1016/j.immuni.2016.02.010

Kurosu, T., Fukuda, T., Miki, T., & Miura, O. (2003). BCL6 overexpression prevents increase in reactive oxygen species and inhibits apoptosis induced by chemotherapeutic reagents in B-cell lymphoma cells. *Oncogene*, *22*(29), 4459-4468. https://doi.org/10.1038/sj.onc.1206755

Kwon, K., Hutter, C., Sun, Q., Bilic, I., Cobaleda, C., Malin, S., & Busslinger, M. (2008). Instructive role of the transcription factor E2A in early B lymphopoiesis and germinal center B cell development. *Immunity*, *28*(6), 751-762. https://doi.org/10.1016/j.immuni.2008.04.014

Lau, C. M., Broughton, C., Tabor, A. S., Akira, S., Flavell, R. A., Mamula, M. J., Christensen, S. R., Shlomchik, M. J., Viglianti, G. A., Rifkin, I. R., & Marshak-Rothstein, A. (2005). RNA-

associated autoantigens activate B cells by combined B cell antigen receptor/Toll-like receptor 7 engagement. *J Exp Med*, *202*(9), 1171-1177. https://doi.org/10.1084/jem.20050630

Leadbetter, E. A., Rifkin, I. R., Hohlbaum, A. M., Beaudette, B. C., Shlomchik, M. J., & Marshak-Rothstein, A. (2002). Chromatin-IgG complexes activate B cells by dual engagement of IgM and Toll-like receptors. *Nature*, *416*(6881), 603-607. https://doi.org/10.1038/416603a

Lee, S. K., Rigby, R. J., Zotos, D., Tsai, L. M., Kawamoto, S., Marshall, J. L., Ramiscal, R. R., Chan, T. D., Gatto, D., Brink, R., Yu, D., Fagarasan, S., Tarlinton, D. M., Cunningham, A. F., & Vinuesa, C. G. (2011). B cell priming for extrafollicular antibody responses requires Bcl-6 expression by T cells. *J Exp Med*, *208*(7), 1377-1388. https://doi.org/10.1084/jem.20102065

Luzina, I. G., Atamas, S. P., Storrer, C. E., daSilva, L. C., Kelsoe, G., Papadimitriou, J. C., & Handwerger, B. S. (2001). Spontaneous formation of germinal centers in autoimmune mice. *J Leukoc Biol*, *70*(4), 578-584. https://www.ncbi.nlm.nih.gov/pubmed/11590194

Nojima, T., Haniuda, K., Moutai, T., Matsudaira, M., Mizokawa, S., Shiratori, I., Azuma, T., & Kitamura, D. (2011). In-vitro derived germinal centre B cells differentially generate memory B or plasma cells in vivo. *Nat Commun*, *2*, 465. https://doi.org/10.1038/ncomms1475

Paus, D., Phan, T. G., Chan, T. D., Gardam, S., Basten, A., & Brink, R. (2006). Antigen recognition strength regulates the choice between extrafollicular plasma cell and germinal center B cell differentiation. *J Exp Med*, *203*(4), 1081-1091. https://doi.org/10.1084/jem.20060087

Phan, R. T., & Dalla-Favera, R. (2004). The BCL6 proto-oncogene suppresses p53 expression in germinal-centre B cells. *Nature*, *432*(7017), 635-639. https://doi.org/10.1038/nature03147

Psianou, K., Panagoulias, I., Papanastasiou, A. D., de Lastic, A. L., Rodi, M., Spantidea, P. I., Degn, S. E., Georgiou, P., & Mouzaki, A. (2018). Clinical and immunological parameters of Sjogren's syndrome. *Autoimmun Rev*, *17*(10), 1053-1064. https://doi.org/10.1016/j.autrev.2018.05.005

Rahman, A., & Isenberg, D. A. (2008). Systemic lupus erythematosus. *N Engl J Med*, *358*(9), 929-939. https://doi.org/10.1056/NEJMra071297

Robinson, M. J., Ding, Z., Pitt, C., Brodie, E. J., Quast, I., Tarlinton, D. M., & Zotos, D. (2020). The Amount of BCL6 in B Cells Shortly after Antigen Engagement Determines Their Representation in Subsequent Germinal Centers. *Cell Rep*, *30*(5), 1530-1541 e1534. https://doi.org/10.1016/j.celrep.2020.01.009

Roco, J. A., Mesin, L., Binder, S. C., Nefzger, C., Gonzalez-Figueroa, P., Canete, P. F., Ellyard, J., Shen, Q., Robert, P. A., Cappello, J., Vohra, H., Zhang, Y., Nowosad, C. R., Schiepers, A., Corcoran, L. M., Toellner, K. M., Polo, J. M., Meyer-Hermann, M., Victora, G. D., & Vinuesa, C. G. (2019). Class-Switch Recombination Occurs Infrequently in Germinal Centers. *Immunity*, *51*(2), 337-350 e337. https://doi.org/10.1016/j.immuni.2019.07.001

Soni, C., Perez, O. A., Voss, W. N., Pucella, J. N., Serpas, L., Mehl, J., Ching, K. L., Goike, J., Georgiou, G., Ippolito, G. C., Sisirak, V., & Reizis, B. (2020). Plasmacytoid Dendritic Cells and Type I Interferon Promote Extrafollicular B Cell Responses to Extracellular Self-DNA. *Immunity*, *52*(6), 1022-1038 e1027. https://doi.org/10.1016/j.immuni.2020.04.015

Sweet, R. A., Christensen, S. R., Harris, M. L., Shupe, J., Sutherland, J. L., & Shlomchik, M. J. (2010). A new site-directed transgenic rheumatoid factor mouse model demonstrates extrafollicular class switch and plasmablast formation. *Autoimmunity*, *43*(8), 607-618. https://doi.org/10.3109/08916930903567500

Sweet, R. A., Ols, M. L., Cullen, J. L., Milam, A. V., Yagita, H., & Shlomchik, M. J. (2011). Facultative role for T cells in extrafollicular Toll-like receptor-dependent autoreactive B-cell responses in vivo. *Proc Natl Acad Sci U S A*, *108*(19), 7932-7937. https://doi.org/10.1073/pnas.1018571108

Toellner, K. M., Gulbranson-Judge, A., Taylor, D. R., Sze, D. M., & MacLennan, I. C. (1996). Immunoglobulin switch transcript production in vivo related to the site and time of antigen-specific B cell activation. *J Exp Med*, *183*(5), 2303-2312. https://doi.org/10.1084/jem.183.5.2303

Vasanwala, F. H., Kusam, S., Toney, L. M., & Dent, A. L. (2002). Repression of AP-1 function: a mechanism for the regulation of Blimp-1 expression and B lymphocyte differentiation by the B cell lymphoma-6 protooncogene. *J Immunol*, *169*(4), 1922-1929. https://doi.org/10.4049/jimmunol.169.4.1922

Victora, G. D., & Nussenzweig, M. C. (2012). Germinal centers. *Annu Rev Immunol*, *30*, 429-457. https://doi.org/10.1146/annurev-immunol-020711-075032

Weening, J. J., D'Agati, V. D., Schwartz, M. M., Seshan, S. V., Alpers, C. E., Appel, G. B., Balow, J. E., Bruijn, J. A., Cook, T., Ferrario, F., Fogo, A. B., Ginzler, E. M., Hebert, L., Hill, G., Hill, P., Jennette, J. C., Kong, N. C., Lesavre, P., Lockshin, M., . . . Nagata, M. (2004). The classification of glomerulonephritis in systemic lupus erythematosus revisited. *J Am Soc Nephrol*, *15*(2), 241-250. https://doi.org/10.1097/01.asn.0000108969.21691.5d

William, J., Euler, C., Christensen, S., & Shlomchik, M. J. (2002). Evolution of autoantibody responses via somatic hypermutation outside of germinal centers. *Science*, *297*(5589), 2066-2070. https://doi.org/10.1126/science.1073924

Wittenborn, T. R., Fahlquist Hagert, C., Ferapontov, A., Fonager, S., Jensen, L., Winther, G., & Degn, S. E. (2021). Comparison of gamma and x-ray irradiation for myeloablation and establishment of normal and autoimmune syngeneic bone marrow chimeras. *PLoS One*, *16*(3), e0247501. https://doi.org/10.1371/journal.pone.0247501

Woodruff, M. C., Ramonell, R. P., Nguyen, D. C., Cashman, K. S., Saini, A. S., Haddad, N. S., Ley, A. M., Kyu, S., Howell, J. C., Ozturk, T., Lee, S., Suryadevara, N., Case, J. B., Bugrovsky, R., Chen, W., Estrada, J., Morrison-Porter, A., Derrico, A., Anam, F. A., . . . Sanz, I. (2020). Extrafollicular B cell responses correlate with neutralizing antibodies and morbidity in COVID-19. *Nat Immunol*, *21*(12), 1506-1516. https://doi.org/10.1038/s41590-020-00814-z

Yokogawa, M., Takaishi, M., Nakajima, K., Kamijima, R., Fujimoto, C., Kataoka, S., Terada, Y., & Sano, S. (2014). Epicutaneous application of toll-like receptor 7 agonists leads to systemic autoimmunity in wild-type mice: a new model of systemic Lupus erythematosus. *Arthritis Rheumatol*, *66*(3), 694-706. https://doi.org/10.1002/art.38298

Zhang, Y., Meyer-Hermann, M., George, L. A., Figge, M. T., Khan, M., Goodall, M., Young, S. P., Reynolds, A., Falciani, F., Waisman, A., Notley, C. A., Ehrenstein, M. R., Kosco-Vilbois, M., & Toellner, K. M. (2013). Germinal center B cells govern their own fate via antibody feedback. *J Exp Med*, *210*(3), 457-464. https://doi.org/10.1084/jem.20120150